INT. J. NUM. METH. HEAT FLUID FLOW, VOL. 4, 229–248 (1994)

HEAT TRANSFER IN DIFFERENTIALLY HEATED NON-NEWTONIAN CAVITIES

K. A. PERICLEOUS

Centre for Numerical Modelling and Process Analysis, University of Greenwich, London SE18 6PF, UK

ABSTRACT

The flow development and heat transfer in a differentially heated cavity containing a non-Newtonian fluid is studied using CFD techniques. Investigations are made for a fluid obeying a power-law type behaviour, for a nominal Rayleigh number of 10^5. Both dilatant and pseudoplastic regimes are considered and the Nusselt number is obtained for a range of power-law index values. The results, given in a graphical and tabular form, suggest that deviations from Newtonian stress–strain behaviour can lead to large changes in overall heat transfer. These changes are due to the behaviour of the wall boundary layers. In the dilatant, or shear-thickening regime, the isothermal wall layers are thick and slow-moving; as a consequence, buoyancy induced flow affects the whole of the cavity volume. In contrast, the pseudoplastic (or shear-thinning) regime leads to thin, fast-moving wall layers whose effect does not propagate to the core of the cavity which remains stagnant. This behaviour, which is directly attributable to the local value of the fluid viscosity, causes the average Nusselt number to decrease with the power-law index, n. Pseudoplastic fluids are therefore better at conducting heat than Newtonian fluids, and conversely dilatant fluids are worse.

The information contained in this paper is of general interest to workers in heat transfer, but is more specifically relevant to researchers in non-Newtonian fluids. Example applications include biotechnology, where close temperature control of bio-cultures in enclosed vessels is required, the food processing industry, the metals casting industry and areas where heat transfer in fine suspensions is required.

KEY WORDS Natural convection Cavity flow Power-law fluids Heat transfer

NOMENCLATURE

a_i	Influence coefficient, cell neighbour i
C_p	specific heat (J/Kg K)
C_ϕ	linearised source coefficient
D	cavity dimension (m)
e_{ij}	strain rate tensor
g	gravity vector (m/s^2)
G	geometric factor and dissipation function
k	consistency coefficient (Ns^n/m^2)
n	power-law index
p	pressure (Pa)
Ra	Rayleigh number ($= g\beta\Delta T D^3\sigma/\nu^2$)
S	source term in conservation equation
t	time (s)
T	temperature (deg C)
u	x-direction velocity component
v	y-direction velocity component
V_ϕ	linearised source boundary value
x	horizontal direction coordinate
y	vertical direction coordinate

Greek symbols

β	coefficient of volume expansion
γ	shear strain rate (s^{-1})
λ	fluid conductivity (W/mK)
μ	dynamic viscosity (kg/ms)
ν	kinematic viscosity (m^2/s)
ρ	density (kg/m^3)
σ	Prandtl number ($= \mu C_p/\lambda$)
τ_0	yield stress (N/m^2)
τ	shear stress (N/m^2)
ϕ	general conserved variable

0961–5539/94/030229–20$2.00

Received May 1993
Revised October 1993

INTRODUCTION

The flow and heat transfer in a differentially heated cavity has been the subject of many investigations within the CFD community. Apart from the obvious practical application (the *double-glazing* example), this problem has been used as a benchmark for testing the accuracy of numerical procedures, differencing schemes and even turbulence models.

The author and his colleagues have contributed in a small way to the plethora of papers on this subject, in a study dealing with a square cavity with differentially heated vertical walls, for a range of Rayleigh numbers between 10^3 and 10^{16} (Reference 2). Jones and de Vahl Davis and Jones produced an early benchmark solution[2,3,4] which many sought to reproduce. Notable in this area is the work of Ostrach, who published a review of the subject in Reference 5. Rather demanding three-dimensional computations have been presented by Mallinson *et al.*[6], for cavities of various aspect ratios, and more recently by Fusegi *et al.*[7] who in addition to convection and diffusion, included thermal radiation in their computations. In most of these calculations the authors have used constant material properties (including density), and a Boussinesq approximation for the buoyancy source driving the flow. However, in some cavity problems the exact prescription of material properties is important, as demonstrated by Reizes *et al.*[8], for the case where the temperature range straddles the density extremum of water. Non-orthogonal grid cavity calculations have been presented by some authors (e.g. Maliska *et al.*[9]) in an attempt to reduce numerical false diffusion. An important class of heated cavity problems involves the onset of instability that leads to a fluctuating temperature field. This situation has been studied successfully by Le Quere *et al.*[10], for a range of cavity aspect ratios.

In contrast to the research activity mentioned in the previous paragraph, the subject of heat transfer in a differentially heated cavity containing non-Newtonian fluids has been poorly researched. This cannot be because the subject is not scientifically stimulating. For example, some recent work has appeared in the literature[11] that demonstrates quite incredibly that the flow can be made to move against gravity in a cavity containing a suitably selected viscoelastic fluid. In fact a literature search will show that the numerical study of heat transfer in non-Newtonian fluids in general is only covered by a handful of publications. Non-Newtonian fluids are however present in a vast range of industries and the problem of what heat transfer coefficient one is to use in heat exchange problems involving such fluids is of great practical importance. Example applications can be found in the biotechnology, biomedicine, food processing and plastic manufacture industries, the petroleum and sewage treatment sectors, the manufacture of nylon fibres, paper, etc. The numerical modelling of complex non-Newtonian flows with heat transfer is now possible, using standard finite-volume, or finite-element techniques[12–15].

The objective of this study is to determine, numerically, the heat transfer coefficient and Nusselt number in a square cavity with differentially heated vertical walls containing a viscous non-Newtonian fluid whose rheology can be characterised by a power-law relation. Computations are performed for a constant nominal Rayleigh number of 10^5, which is in the laminar regime. Both dilatant (or shear-thinning) and pseudoplastic (shear-thickening) fluids are simulated by suitably varying the power-law index in the rheology model. The results are compared with the Newtonian case that is used as a benchmark.

In the chapters that follow, the test-case modelled is first described in detail, the mathematical model used is then explained, the results of the computations are described and the salient features of this kind of flow highlighted. The main conclusions of this work and suggestions for future study complete the main body of the report, followed by a list of references and figures.

THE PROBLEM CONSIDERED

The physical problem simulated concerns a square cavity, which is differentially heated along its vertical walls. The horizontal top and bottom walls are adiabatic. The cavity is assumed to

be of infinite depth in the third dimension. The temperature difference across the cavity is 20°, with the left wall being *hot* and the right wall being *cold.*

The dimension, D, of the cavity sides was chosen to give the desired Rayleigh number. Therefore, for Ra equal to 10^5, $D = 0.0363$ m. Laminar wall friction is assumed to apply on all walls. Heat transfer through the walls causes density changes to the fluid in the cavity, and leads to buoyancy driven recirculation. The resulting flow is assumed to be steady and, at the chosen Rayleigh number, laminar[1]. The fluid within the cavity is assumed to obey a power-law stress–strain relationship.

FLOW EQUATIONS

The equations describing the flow are governed by the laws of conservation of mass, momentum and energy. In addition constitutive relationships are needed to close these equations; these describe point properties of the fluid such as density, viscosity, conductivity etc. and their relationship to the problem dependent variables. The conservation equations can be expressed in a generalised form that is amenable to algorithmic treatment and is common to most CFD techniques. Hence, the transport of a conserved variable ϕ, is given in the following form:

$$\underbrace{\underset{\text{accum. rate}}{\frac{\partial \rho\phi}{\partial t}} + \underset{\text{convection}}{\operatorname{div}(\rho u\phi)} - \underset{\text{diffusion}}{\Gamma_\phi \nabla\phi}}_{\text{efflux per unit volume}} = \underset{\text{source}}{S_\phi} \tag{1}$$

When ϕ is equal to 1, the mass continuity equation is returned, whilst for momentum the three velocity components (u, v, w) appear and enthalpy is used to describe thermal energy transport. It will be noted that the pressure does not appear independently as the subject of a conservation equation. It is however used in an iterative correction scheme known as SIMPLEST[16] to ensure momentum and mass conservation is ultimately satisfied simultaneously.

The diffusion coefficient Γ appearing in (1), represents the influence of diffusion in the transport of ϕ. In non-Newtonian flows, Γ becomes the fluid *apparent* viscosity, which is a function of local shear rate and possibly other problem variables.

In two-dimensional Cartesian form, equation (1) expands to the following:

Continuity

$$\frac{\partial \rho}{\partial t} + \frac{\partial}{\partial x}(\rho u) + \frac{\partial}{\partial y}(\rho v) = 0 \tag{2}$$

x-Momentum

$$\rho\left(\frac{\partial u}{\partial t} + u\frac{\partial u}{\partial x} + v\frac{\partial u}{\partial y}\right) = -\left[\frac{\partial}{\partial x}(\tau_{xx}) + \frac{\partial}{\partial y}(\tau_{yx})\right] - \frac{\partial p}{\partial x} + \rho g_x \beta(T - T_{ref}) \tag{3}$$

v-Momentum

$$\rho\left(\frac{\partial v}{\partial t} + u\frac{\partial v}{\partial x} + v\frac{\partial v}{\partial y}\right) = -\left[\frac{\partial}{\partial x}(\tau_{xy}) + \frac{\partial}{\partial y}(\tau_{yy})\right] - \frac{\partial p}{\partial y} + \rho g_y \beta(T - T_{ref}) \tag{4}$$

where ρ is the density and τ_{ij} is the dynamic stress tensor. Also,

$$\tau_{ij} = -\mu e_{ij} \tag{5}$$

where μ is the viscosity and e_{ij} the rate of strain tensor. The components of τ_{ij} and e_{ij} are readily available in the literature, e.g. Reference 17.

To compare against the benchmark results of References 2 and 3, the density was presumed to be constant in this calculation. The buoyancy force in the momentum equations is represented

instead by the Boussinesq approximation (last term in equations (3) and (4)), which substitutes density variations with variations about the reference temperature, multiplied by the coefficient of thermal volume expansion, β. Gravity is then given by the vector components g_x and g_y. This approximation is a reasonable one to adopt, provided the temperature range about the mean is small, as is true here (see Markatos[1]).

Energy equation

$$\rho Cp\left(\frac{\partial T}{\partial t} + u\frac{\partial T}{\partial x} + v\frac{\partial T}{\partial y}\right) = \lambda\left[\frac{\partial^2 T}{\partial x^2} + \frac{\partial^2 T}{\partial y^2}\right] + \mu G \tag{6}$$

where λ is the conductivity of the fluid and Cp the specific heat.

The last term on the RHS of (7) represents heating due to viscous dissipation of energy. The quantity G represents the second invariant of the rate of strain tensor, e_{ij} and it is also known as the dissipation function.

$$G = 2\left[\left(\frac{\partial u}{\partial x}\right)^2 + \left(\frac{\partial v}{\partial y}\right)^2\right] + \left(\frac{\partial v}{\partial x} + \frac{\partial u}{\partial y}\right)^2 \tag{7}$$

Representation of the viscosity

In Newtonian fluids, the viscosity appearing in (5) above is, of course, a constant. However, in the case considered here, this is not true. The dynamic stress tensor and the strain rate are related to each other non-linearly, in a way that is often difficult to determine experimentally. It is then useful to talk of the apparent viscosity of the fluid, defined as the ratio of shear stress to shear strain. Provided this is independent of the amount of deformation and its duration, then following Metzner's[18] classification the fluid is called purely viscous. Purely viscous fluids are considered in this investigation, namely, (a) shear thinning (pseudoplastic), (b) shear thickening (dilatant). For the cases described, the generalised Bingham, or Herschel–Buckley[17] equation is adopted, i.e.:

$$\tau = \tau_0 + k\gamma^n \tag{8}$$

where

τ is the shear stress (N/m^2)
τ_0 is the yield stress (N/m^2)
k is the consistency coefficient (Ns^n/m^2)
n is the consistency index, and
γ is the shear strain rate (s^{-1})

For plastics and other very viscous fluids, the consistency index is usually a function of temperature. An Arrhenius expression was used in Pericleous and Akay[12] to represent this dependence. Hence,

$$k = k_0 \exp\left[\frac{\Delta E}{R_c}\left(\frac{1}{T} - \frac{1}{T_0}\right)\right] \tag{9}$$

where k_0 is constant, ΔE the flow activation energy (cal/mole), R_c the gas constant and T_0 the reference temperature.

Equation (8) reduces to the power law relation when the yield stress is zero. Then, if $n = 1$ it represents a *Newtonian* fluid, $n < 1$ a *pseudoplastic*, and $n > 1$ a *dilatant* non-Newtonian fluid. *Figure 1* shows computed velocity profiles in a circular pipe, when there is no yield stress. The Newtonian laminar parabolic profile becomes broader when $n = 0.5$, and conversely elongated when $n = 1.5$. *Figure 2* shows what happens when a finite yield stress $y = 10\ N/m^2$ is introduced. A plug flow region is predicted in the central region of the pipe, where the fluid behaves as a translating solid or alternatively as a fluid of infinite viscosity. For this simple example, computed results agree perfectly with analytical solutions (see also Pericleous and Patel[15]).

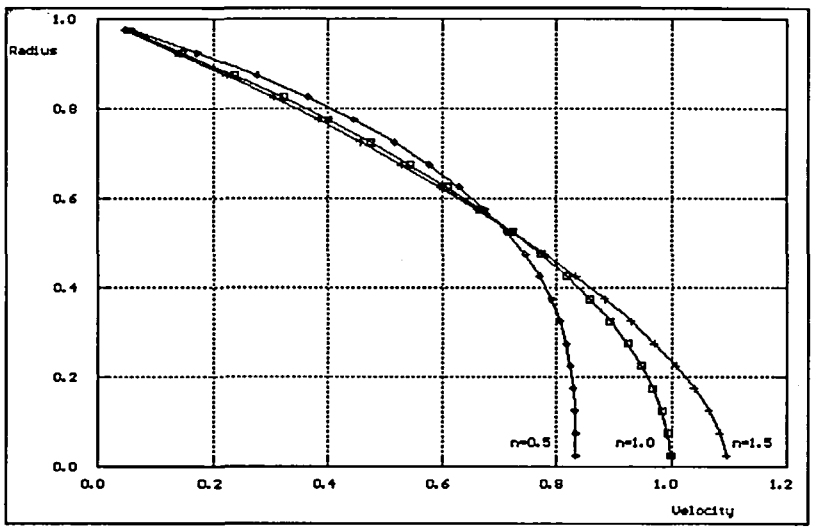

Figure 1 Power-law flow in a pipe

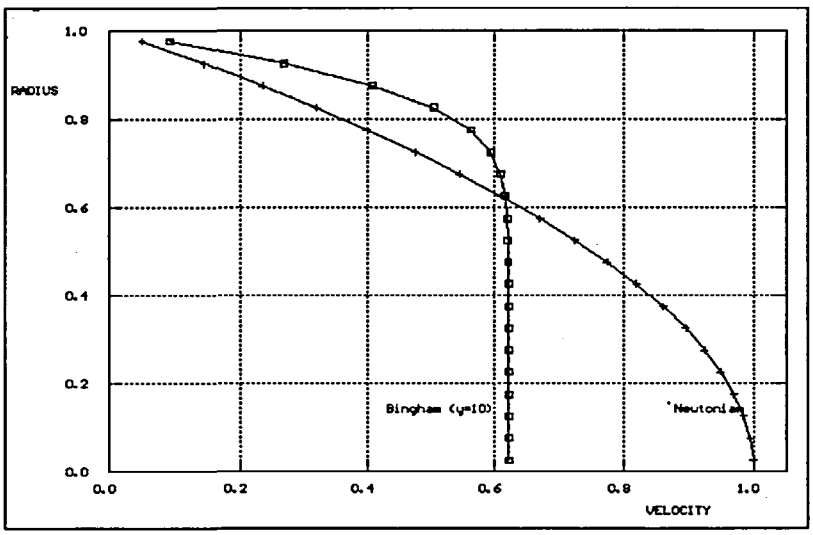

Figure 2 Bingham flow in a pipe

The apparent viscosity, μ_{app}, used in the computations is derived from equation (8), after dividing through by γ. Hence,

$$\mu_{app} = \frac{\tau}{\dot{\gamma}} = \frac{\tau_0}{\dot{\gamma}} + k\dot{\gamma}^{(n-1)} \tag{10}$$

This equation becomes ill-conditioned, since as $\gamma \to 0$, $\mu_{app} \to \infty$. Numerical problems may arise in an iterative computational scheme, due to a large and very abrupt change in apparent viscosity between the yielding and non-yielding regions of the fluid. To avoid these, the apparent viscosity

is derived from the following equation:

$$\tau = \left(\frac{\tau_0}{\dot{\gamma}^*} + k\dot{\gamma}^{*(n-1)}\right)\dot{\gamma} = \mu_{app}\dot{\gamma} \tag{11}$$

where the starred quantity refers to the previous iteration value. However, the calculated shear stress and strain rate, must still satisfy equation (10), *not* (11). Hence, following Maeda[13] the following iteration scheme is adopted:

(a) Use the stored viscosity to evaluate the tentative velocity field, by solving equations (1)–(4).
(b) Evaluate the resulting strain rate, from (7) ($\gamma = G^{0.5}$).
(c) Calculate the "pseudo-strain rate", γ^*, from (10).
(d) Calculate the new apparent viscosity value, from (11) and repeat steps (a)–(d).

This scheme works particularly well when the initial yield stress is finite.

Boundary conditions are needed for problem closure. These occupy the source term S_ϕ in RHS of the equations. The appropriate sources for the heated cavity are given in *Table 1*. Reference property values are then evaluated at the average temperature, $T_{ref} = 0$, as shown in *Table 2*.

Table 1 Boundary conditions

Boundary/variable	T	u	v
Hot wall; $x = 0$	$T = +10$	$u = 0$	$\tau_w = -\mu\, dv/dx$
Cold wall; $x = D$	$T = -10$	$u = 0$	$\tau_w = -\mu\, dv/dx$
Top wall; $y = D$	$dT/dy = 0$	$\tau_w = -\mu\, du/dy$	$v = 0$
Bottom wall; $y = 0$	$dT/dy = 0$	$\tau_w = -\mu\, du/dy$	$v = 0$

Table 2 Reference properties

Property	Value
Density, ρ	1.207
Prandtl no, σ	0.71
Nominal kinematic viscosity, ν	1.56×10^{-5}
Volume expansion coefficient, β	1/273

Table 3 Summary of findings

Run no.	Index, n	V_{max} (m/s)	δx (m)	$\gamma(y = D/2)$	Nusselt no. $\langle Nu \rangle$	Q_{wall} (W)
0	cond.	0.0	–	0.0	1.0	5.304E – 4
1	0.1	0.091	0.0008	113.75	8.04	4.266E – 3
2	0.25	0.082	0.0008	102.50	7.14	3.790E – 3
3	0.5	0.069	0.0011	62.73	6.40	3.400E – 3
4	0.75	0.054	0.0017	31.76	5.47	2.900E – 3
5	1.0	0.042	0.0025	16.80	4.56	2.418E – 3
6	1.25	0.033	0.0030	11.00	3.93	2.086E – 3
7	1.5	0.028	0.0036	7.78	3.50	1.854E – 3
8	1.75	0.024	0.0041	5.85	3.18	1.690E – 3
9	2.0	0.022	0.0047	4.79	2.95	1.568E – 3

SOLUTION PROCEDURE

The conservation equations are solved in a discretised form on a Cartesian solution grid. The problem dependent variables and fluid properties are assumed constant within a grid cell. A staggered convention is used, whereby all scalars are located in the cell centre while velocities reside on the appropriate cell face. Integration of the PDE's (1)–(6) over the elemental control volumes defined by each cell leads to a set of finite difference equations, or FDE's. These are linear expressions relating the variable Φ to all its neighbours in space and its previous time value through influence coefficients, which provide convective and diffusive links. Hence,

$$\Phi = \frac{\sum a_i \Phi_i + C_\Phi V_\Phi G}{\sum a_i + C_\Phi G} \tag{12}$$

The terms C_Φ and V_Φ represent the *coefficient* and *value* of the linearised source S_Φ that can be expressed as:

$$S_\Phi = C_\Phi (V_\Phi - \Phi) G \tag{13}$$

where Φ is the resident cell value and G a geometrical factor.

Although equation (12) is linear in form, the influence coefficients of variable Φ, are not constants but functions of the other variables solved. This means the solution has to be procured iteratively. Such an iterative procedure is embodied in the code PHOENICS[20], used in this simulation, in the form of the SIMPLEST[16] algorithm, in which a guess-and-correct approach is followed to ensure that once a velocity field has been guessed, pressure corrections lead to continual adjustment of this field until continuity is satisfied and error residuals in all dependent variable equations fall below predefined thresholds.

There are important differences between SIMPLE, the original pressure correction scheme by Patankar and Spalding[19] and Spalding's SIMPLEST; the latter has better convergence characteristics for this type of problem, where both convective and diffusive contributions to the momentum equations are important. The differences between the two techniques are discussed in Reference 1 and in greater detail in Reference 16. A hybrid interpolation scheme is adopted in the formulation of the influence coefficients in equation (12).

The iteration process is deemed to be *converging* when the residuals in successive sweeps are diminishing. The speed with which convergence is achieved depends on many factors, including the extent to which variables influence each other and the realism of the initial guessed fields. Convergence control is exerted via the use of an inertial under-relaxation term, which acts as a false time step in the equations. Inertial under-relaxation can be thought of as an additional source term S, say, which appears in each FDE. Therefore,

$$S_r = \frac{\rho}{\partial t_f} (\Phi^* - \Phi) Vol \tag{14}$$

where Φ^* represents the value of Φ at the previous iteration, ρ is the fluid density, δ_{tf} the false time step and Vol the cell volume. It is evident by examining equation (12), that as the coefficient of this source becomes large (by making δ_{tf} small) the value of Φ will remain close to that at the previous iteration, Φ^*. Furthermore, as the solution converges $\Phi \rightarrow \Phi^*$ and $S_r \rightarrow 0$, ensuring that the relaxation term does not affect the final solution.

Typically 300 iterations of the coupled set of equations were necessary to reach convergence for each run performed, starting from uniform initial conditions. This number could be significantly reduced, if the computation started from the stored solution of a parametrically related previous run. No particular convergence problems were encountered and the residual errors diminished monotonically in all the cases presented here. Slightly heavier relaxation was necessary in the pseudoplastic set of runs, for best convergence. The reason for this, as seen in the results, is due to an increase in the local Rayleigh number characterising the wall layers,

due to shear thinning. As noted in our previous work on Newtonian cavities[1], convergence becomes progressively more difficult to achieve as the Rayleigh number increases, because the coupling of the energy and momentum equations becomes stronger.

A moderately fine 40 × 40 grid was used for all the simulations. The grid was made finer close to the walls and coarser in the middle of the cavity, following the practice of Reference 1. The code PHOENICS was used for all the computations presented. The author developed a Fortran attachment to PHOENICS, that contains the non-Newtonian model.

RESULTS AND DISCUSSION

Table 3 gives a list of the cases and a summary of the main findings. It includes the controlling parameter n, in column two, the maximum vertical velocity in the boundary layer (at $D/2$) its distance from the wall, the corresponding strain-rate, the average Nusselt number and the overall heat transfer through the cavity. Run no. 5 in the table corresponds to the Newtonian case.

It is immediately obvious from the table, that as the power-law index increases from 0.1 to 2.0, there is a corresponding decrease in the amount of thermal energy transferred across the cavity. It also appears from the table, that the maximum vertical velocity and strain rate diminish as n increases and the boundary layer thickens.

The average Nusselt number, defined as $\langle \mathrm{Nu} \rangle = h_c D/\lambda$, is the quantity of interest from the engineering point of view, as it describes the convective heat transfer coefficient, h_c, for the rate of heat flow across the cavity. Column seven in *Table 3* gives the total heat transfer for all cases studied, and for a hypothetical situation where only conduction is allowed in the cavity. Column six then, gives the average Nusselt number which has been deduced from the following equation:

$$\langle \mathrm{Nu} \rangle = Q_{wall}/(\lambda \Delta T) \tag{15}$$

The Nusselt number for conduction only, has a value of 1.0, by definition. Values greater than one denote the convective contribution to heat transfer. As noted in the previous paragraph, heat transfer decreases with the power-law index n, and as a consequence of equation (15), the average Nusselt number also decreases. The value of $\langle \mathrm{Nu} \rangle$ for $n = 1.0$ agrees well with the benchmark solutions given in the literature (e.g. 4.519 in de Vahl Davis[3], compared to 4.56 here). The dependence of the Nusselt number on the power-law index is also shown in *Figure 3*.

Detailed results are given graphically, in *Figures 4–10*. The figures containing contours are grouped in sets of five (in order of diminishing n) and depict velocity vectors and temperature contours. *Figures 4(a)* to *4(e)* first show velocity vectors in the cavity. The general clockwise recirculation induced by buoyancy can be seen quite clearly in all cases, with the hot thermal layer flowing upwards and counteracted by the cold thermal layer which flows downwards along the opposite wall. The flow field shows rotational symmetry as expected. There are large changes in the thickness of the wall boundary layers, accompanying change in the power-law index. The boundary layers become thinner (and faster), as the fluid changes from dilatant to Newtonian and then to pseudoplastic. At the same time, as the flow activity concentrates close to the walls, the low-velocity central region of the cavity expands, until at the highly shear-thinning $n = 0.1$, the whole of the central region becomes stagnant. Observing more closely the central region, we note that the initial vortex of *Figure 4(a)*, becomes elongated and breaks into two distinct vortices which move along the cavity diagonal, towards the downstream end of the thermal boundary layers (*Figures 4(b)* and *4(c)*). *Figure 4(c)* corresponds to the Newtonian result, and the flow behaviour is familiar to us from previous references[1–4]. As the fluid becomes pseudoplastic, the two vortices move further along the diagonal, until at the extreme values of the index, $n < 0.25$, the flow behaviour changes significantly. Separation regions develop at the downstream corners of the adiabatic walls, containing counter-clockwise vortices. At the same time, a very weak central vortex appears; this is accompanied by a shift in the location of the diagonal vortices, which suddenly switch diagonal.

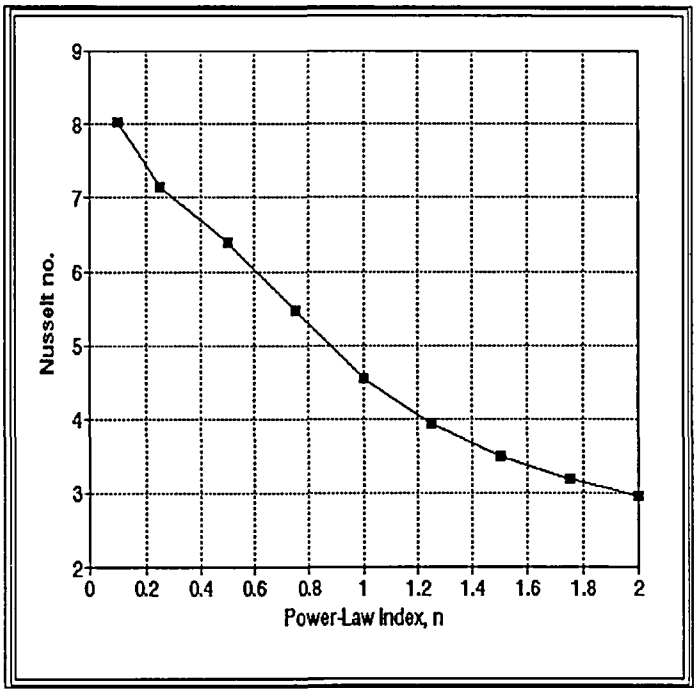

Figure 3 Effect of power-law index on Nusselt number

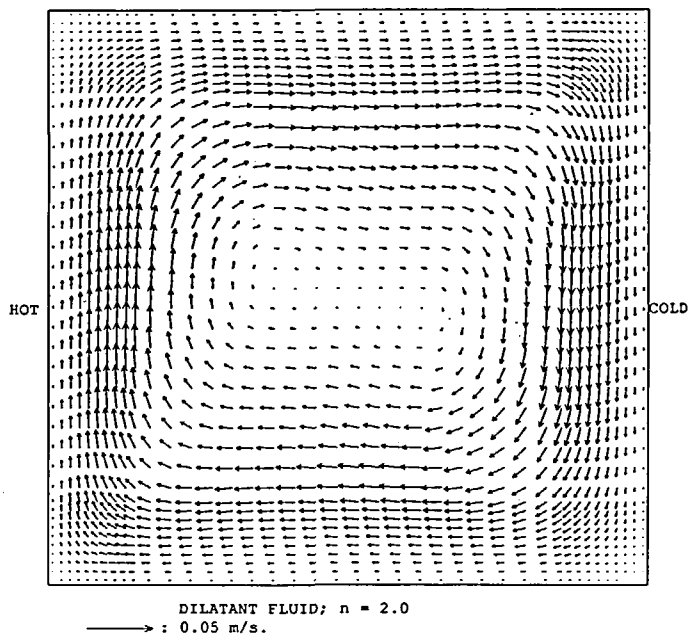

(a)

Figure 4 Velocity vectors: (a) $n = 2.0$

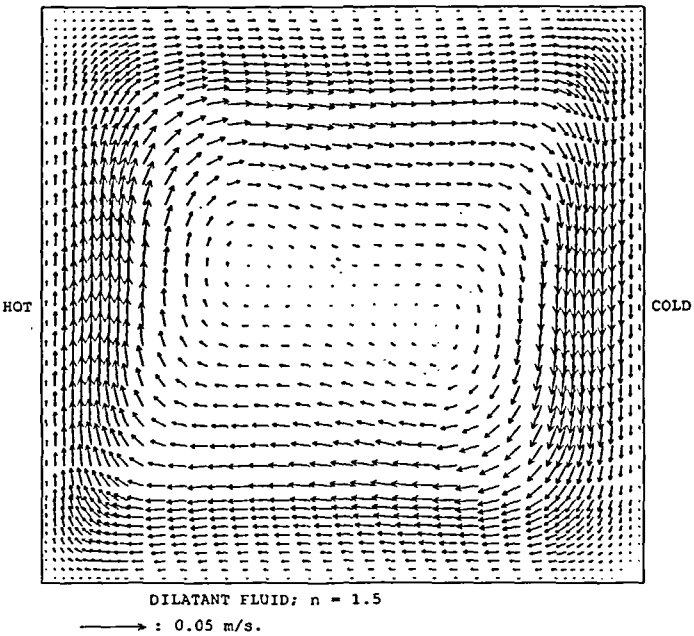

(b)

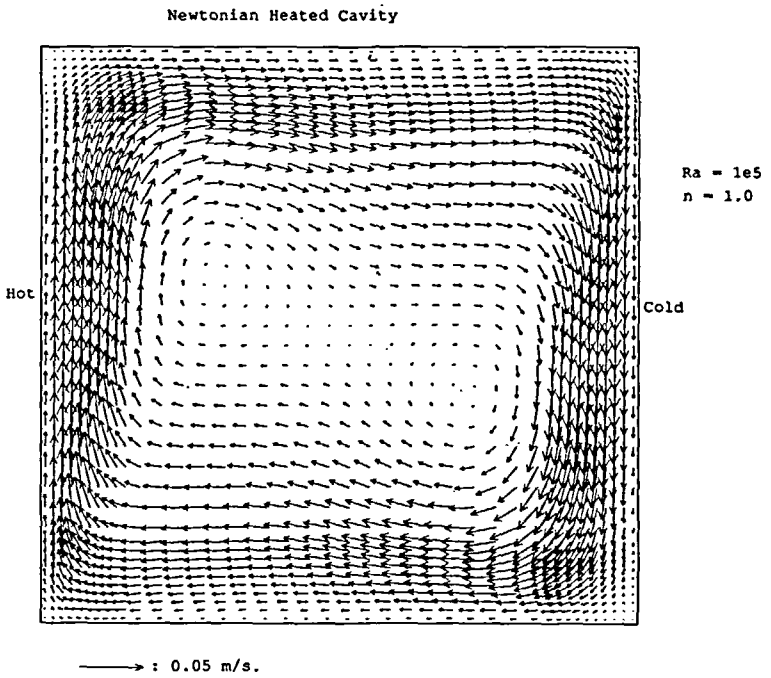

(c)

Figure 4 (b) $n = 1.5$; (c) $n = 1.0$

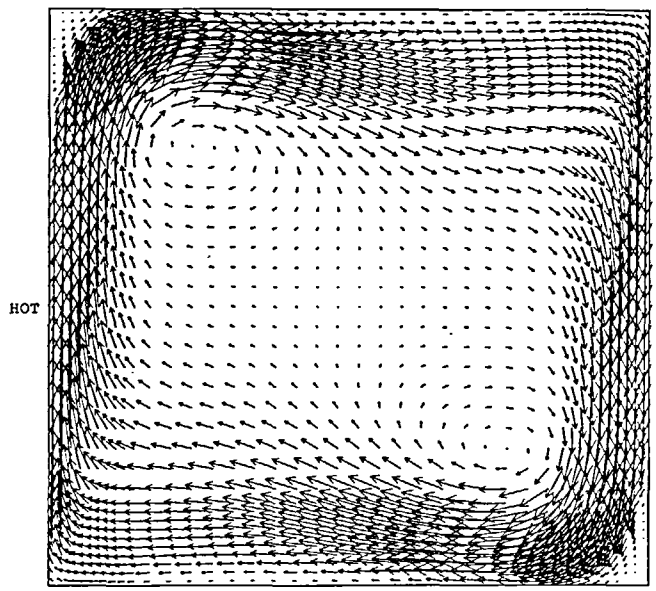

(d)

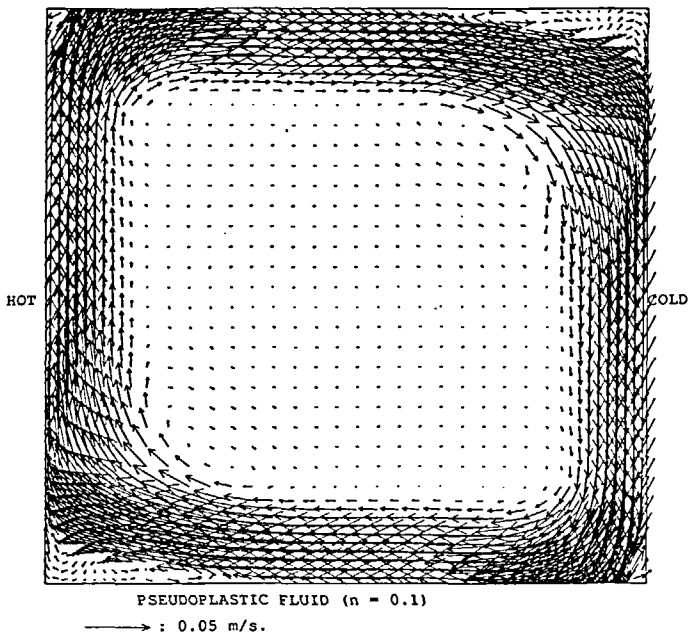

(e)

Figure 4 (d) $n = 0.5$; (e) $n = 0.1$

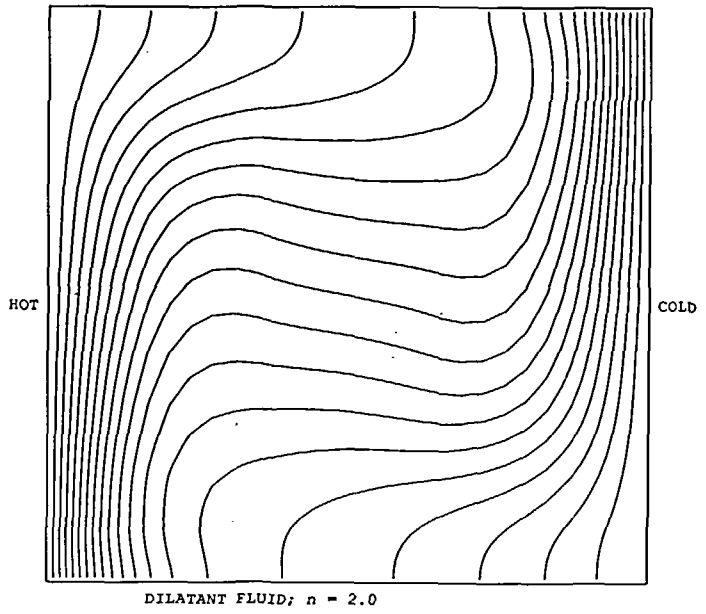

(a)

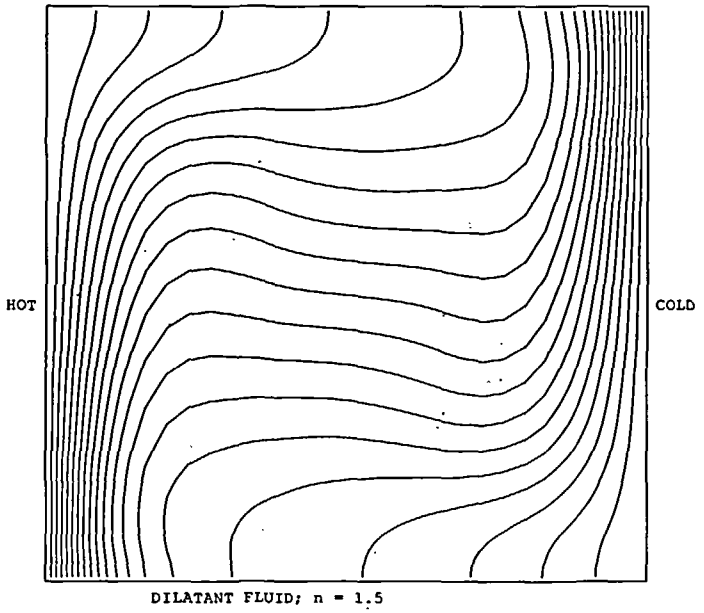

(b)

Figure 5 Temperature contours $-10(1)10$: (a) $n = 2.0$; (b) $n = 1.5$

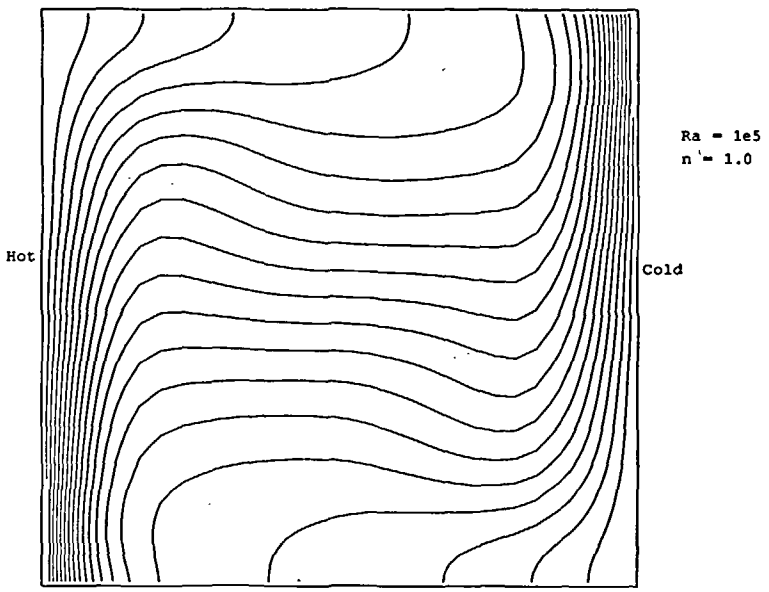

(c)

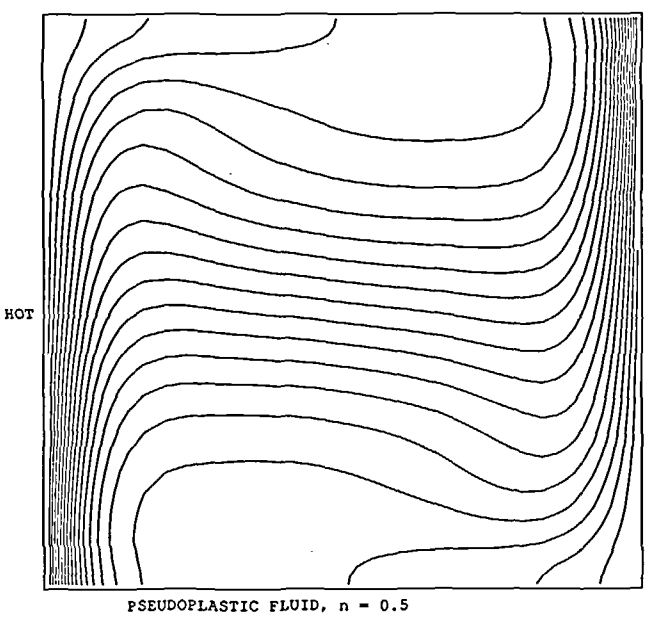

(d)

Figure 5 (c) $n = 1.0$; (d) $n = 0.5$

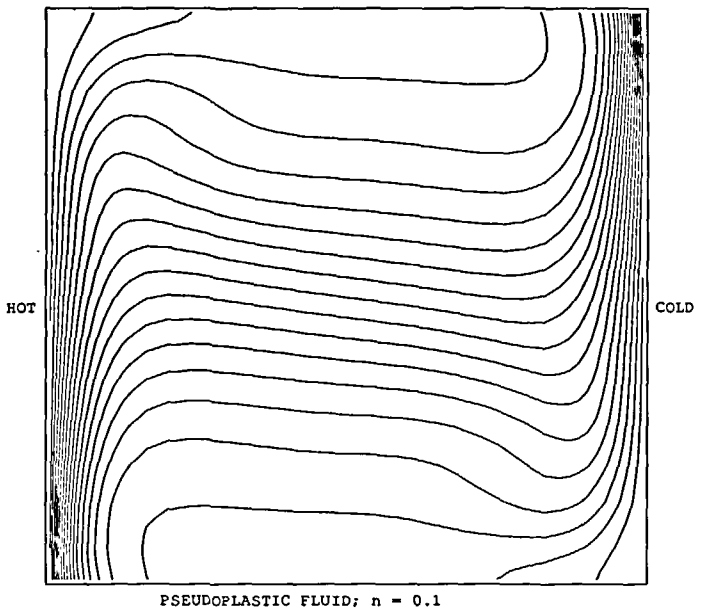

(e)

Figure 5 (e) $n = 0.1$

Figures 5(a) to *5(e)* show the corresponding temperature field. Contour lines are given at one degree intervals. In pure conduction, one would expect temperature contour lines to be parallel to the isothermal walls of the cavity, since there is no heat transfer at the top and bottom walls. Convection modifies this tendency, as hot fluid carried upwards from the heated wall mixes with lower temperature fluid towards the top of the cavity, and in reverse cold fluid is carried downwards along the cold wall, to mix with higher temperature fluid towards the bottom of the cavity. As a result, the contour lines approach the horizontal in the central region of the cavity, until the temperature gradient actually changes sign. This change of sign induces vorticity in the flow which resists the clockwise rotation of the fluid, leading to the elongation and break-up of the central vortex. As in the vector plots, the extent of the central region behaviour expands with diminishing power-law index. *Figure 5(c)* corresponds to the Newtonian case, where the central region now shows evidence of stratification, with colder, heavier, fluid lying in the bottom half of the cavity and lighter, warmer fluid occupying the top half. As the fluid becomes more pseudoplastic this trend continues. In addition, the temperature gradients close to the isothermal walls become steeper, as the boundary layers becoming thinner. The stratification is maintained by thin discharge jets emanating from the hot and cold walls which now penetrate a long way along the isothermal walls.

The overall flow behaviour is perhaps best seen in the streamline plots in *Figures 6(a)–(6f)*, which in this case correspond to $n = 0.25, 0.5, 0.75, 1.0, 1.25$ and 1.75 respectively. The break-up of the initial central vortex and the separation of the two successors as n diminishes is the most obvious feature of these plots. At the same time fluid activity concentrates more-and-more towards the walls as seen by the concentration of the stream function contour lines. This is because the viscosity becomes progressively higher in the central region and lower close to the walls. *Figure 6(a)*, for $n = 0.25$ shows the two effects commented upon earlier, i.e. the appearance of a weak central vortex, accompanied by a shift of the diagonal vortex-pair position.

The viscosity behaviour can be best understood with reference to *Figure 7(a)* and *7(b)*, which depict line plots of viscosity ratio (μ/k_0) along the vertical and horizontal cavity mid-planes

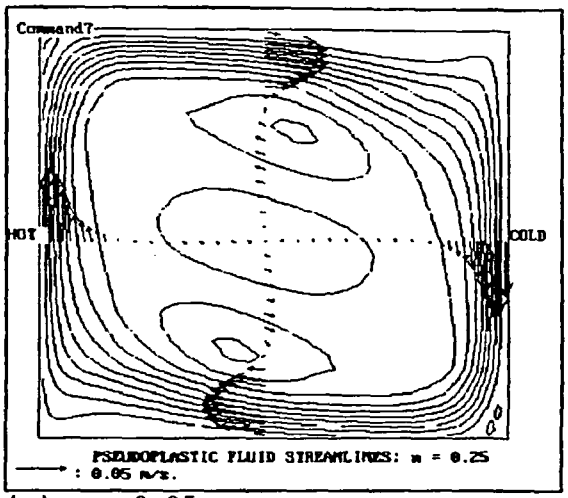

(a) n = 0.25

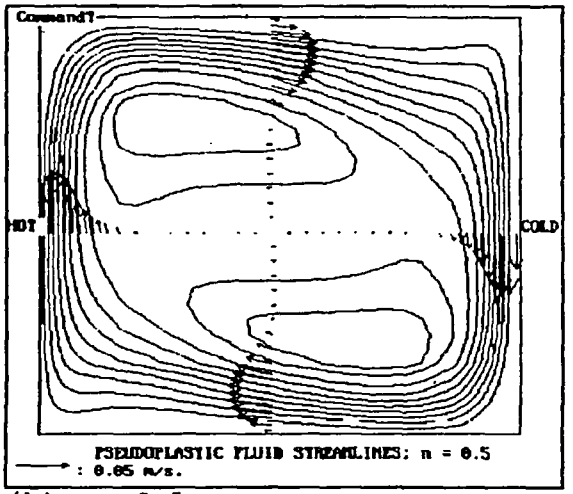

(b) n = 0.5

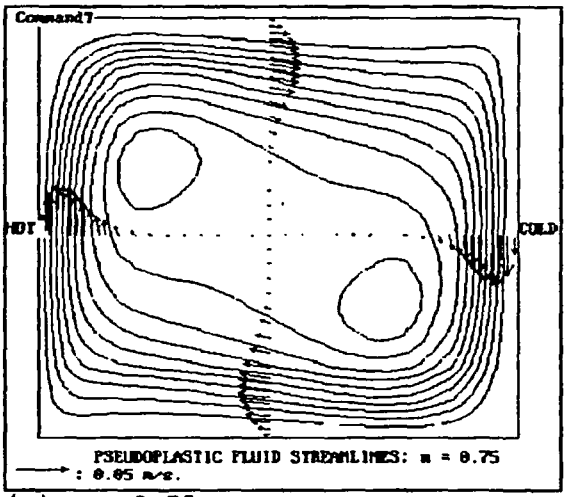

(c) n = 0.75

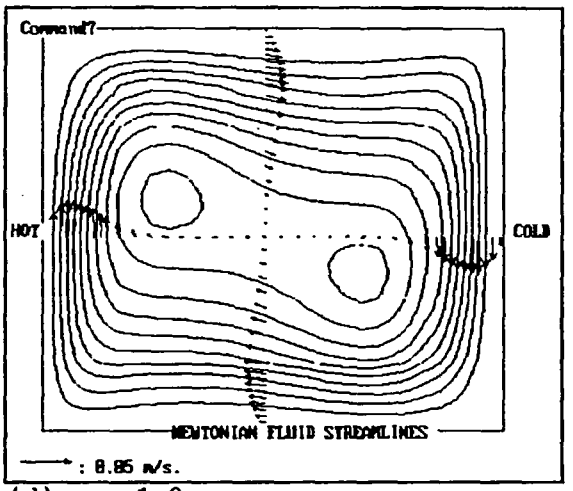

(d) n = 1.0

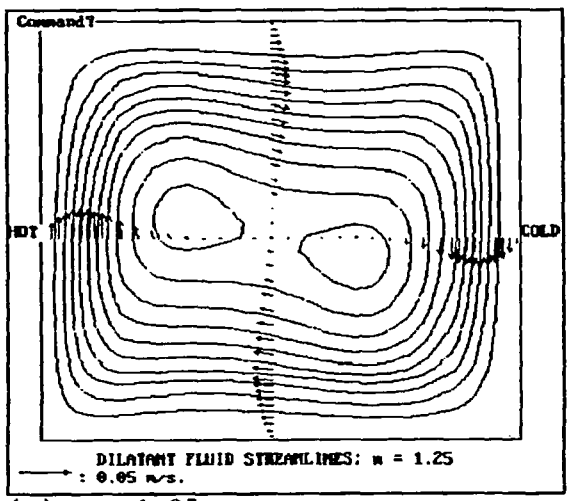

(e) n = 1.25

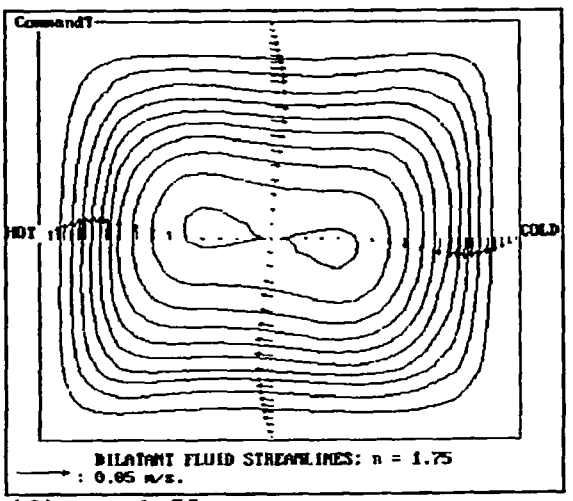

(f) n = 1.75

Figure 6 Flow streamlines – effect of power-law index: (a) $n = 0.25$; (b) $n = 0.5$; (c) $n = 0.75$; (d) $n = 1.0$; (e) $n = 1.25$; (f) $n = 1.75$

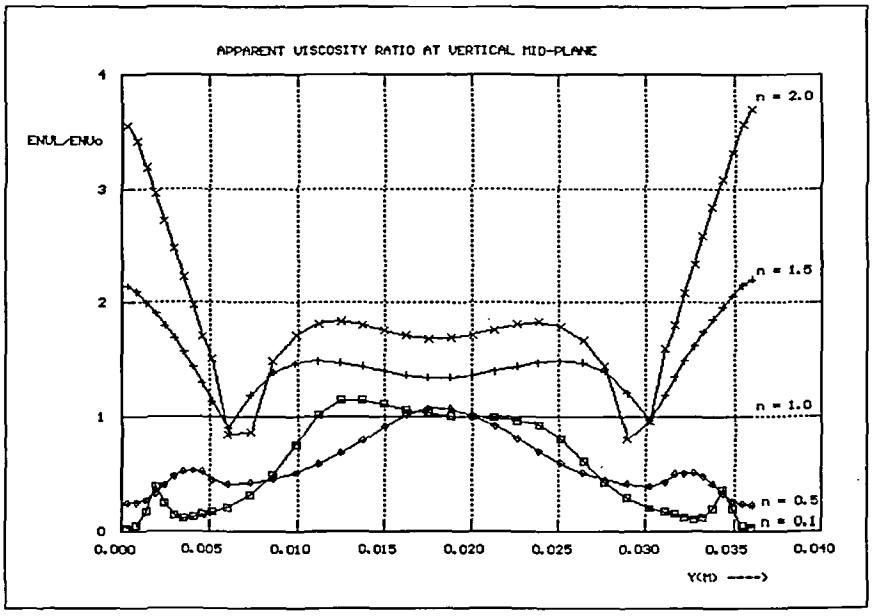

(a)

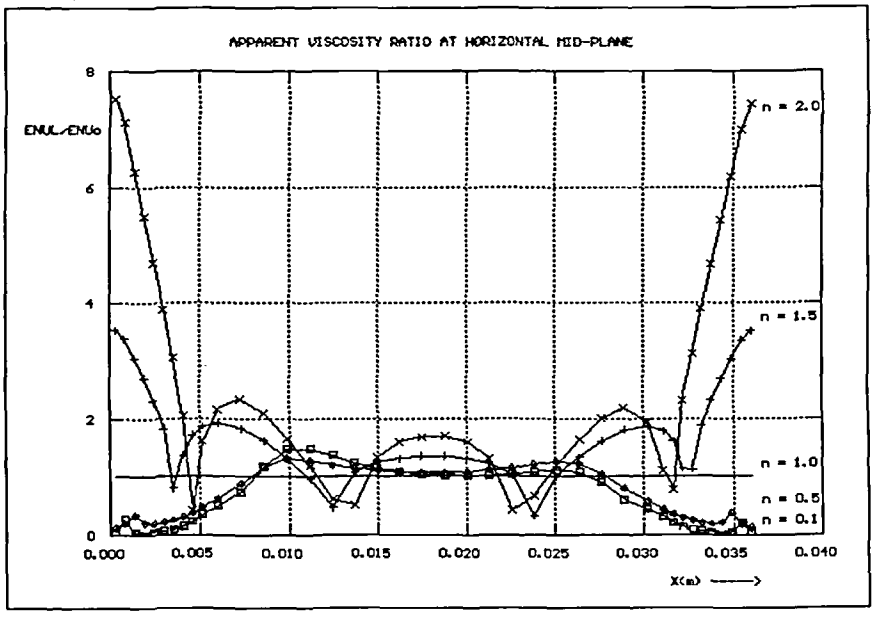

(b)

Figure 7 Apparent viscosity ratio along selected sections: (a) vertical mid-plane; (b) horizontal mid-plane

respectively, for various values of the power-law index n. The ratio is of course constant for the Newtonian case ($n = 1.0$). Generally speaking, close to the wall, the pseudoplastic fluid has a viscosity ratio which is less than one, and conversely the dilatant fluid a viscosity ratio which is substantially greater than one; this trend is more pronounced at the extremes of the power-law index. In the cavity core, the viscosity is at a maximum in the pseudoplastic fluid and at a minimum in the dilatant. This behaviour is a direct consequence of the power-law model used, and it reflects the strain-rate variation in the cavity. As the strain-rate approaches zero, the viscosity becomes very large if $n - 1 < 0$ and small if $n - 1 > 0$.

The viscosity plots also help to explain the overall flow behaviour in the cavity. In the dilatant regime, the viscosity tends to be highest in regions of fluid activity. Since the Rayleigh number is inversely proportional to the viscosity, this implies that the local value of the Rayleigh number is lower than the nominal. Since the overall behaviour of the cavity is governed by what happens in the high activity regions (i.e. the boundary layers) the cavity behaves in some respects like a Newtonian cavity of *lower* Rayleigh number. Quite the opposite happens in the pseudoplastic regime; there, the viscosity is low in the boundary layers, hence the local Rayleigh number is high. The pseudoplastic cavity therefore behaves like a Newtonian cavity, of *higher* Rayleigh number. Inspection of the velocity and temperature plots and comparison against Newtonian results (for example, Reference 1) quickly demonstrates this analogy.

The overall heat transfer (given by the Nusselt number) also follows the analogy suggested above. Heat transfer *increases* with decreasing power-law index, in the direction of *increasing* local Rayleigh number. This is because the rate of fluid transport in the boundary layers (hence the heat convected) increases as the power-law index diminishes, as the boundary layers become thinner but faster. The velocity and thermal boundary layers at the isothermal walls can be seen in *Figures 8* and *9* showing profiles at the cavity horizontal mid-plane. *Figure 10* shows the corresponding horizontal velocity along a vertical mid-plane.

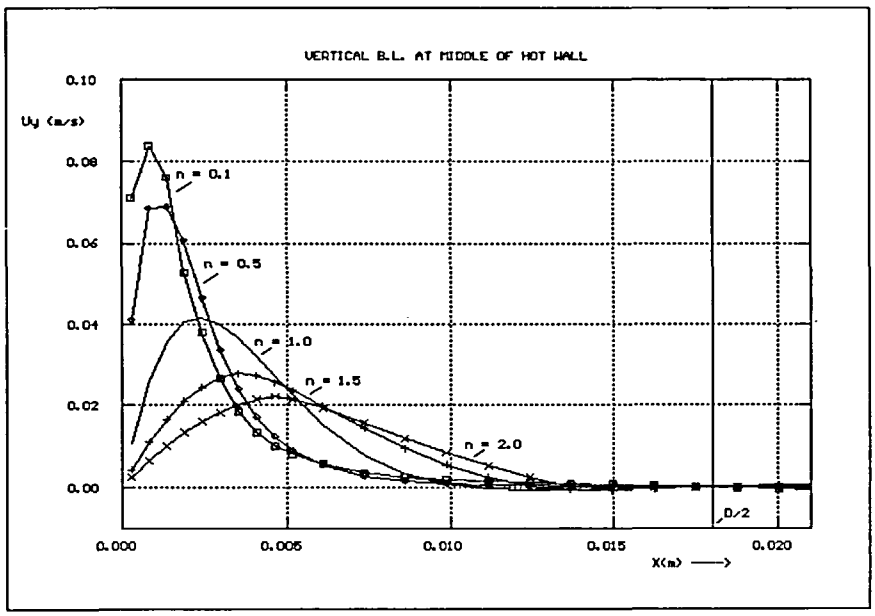

Figure 8 Vertical velocity distribution at mid-plane between adiabatic walls

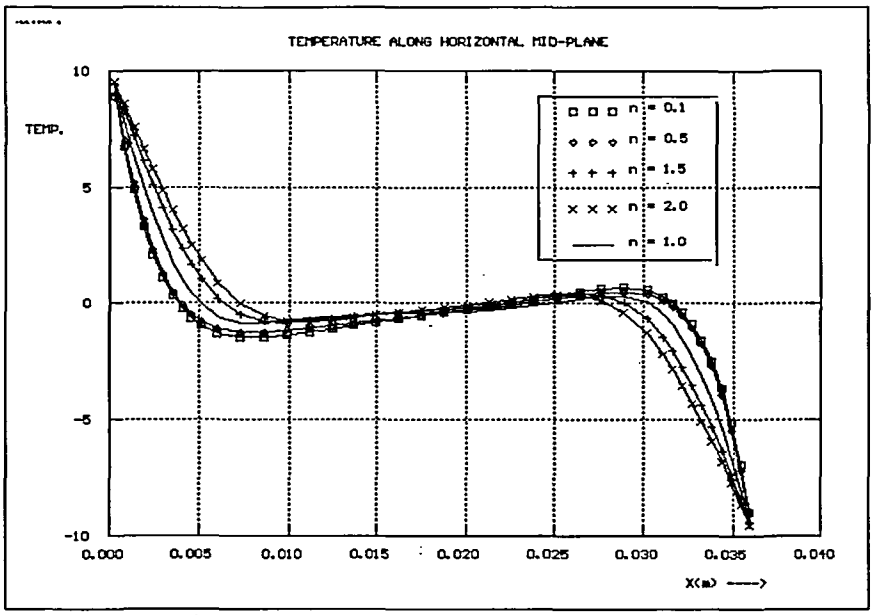

Figure 9 Temperature distribution at mid-plane between adiabatic walls

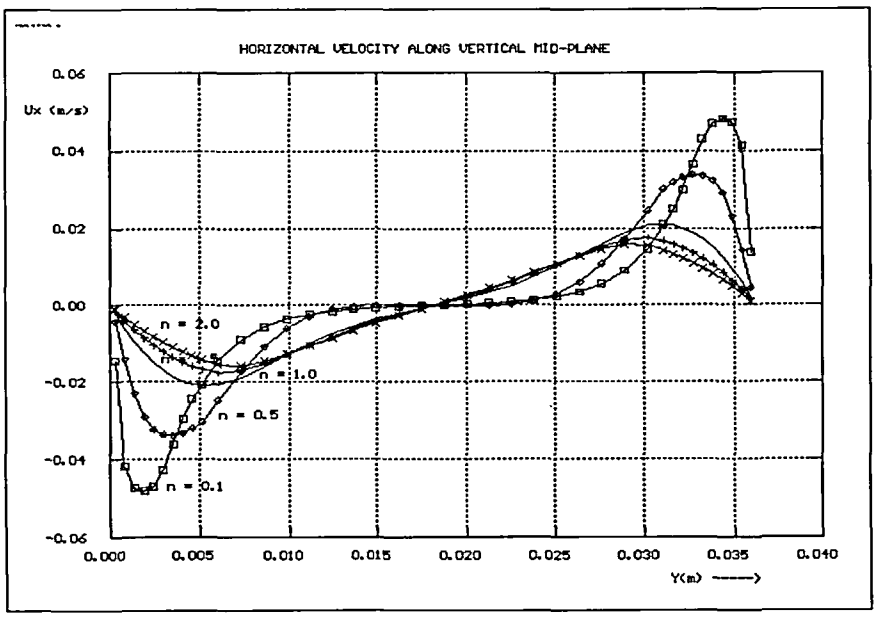

Figure 10 Horizontal velocity distribution at mid-plane between isothermal walls

CONCLUSIONS

This work demonstrates the use of CFD techniques to the problem of natural convection in a differentially heated cavity, containing a non-Newtonian fluid. The fluid obeys a power-law type stress-strain relationship.

Parametric computations were performed for a range of power-law index values covering both dilatant and pseudoplastic flow regimes and the results were compared against the Newtonian benchmark solution, at a Rayleigh number equal to 10^5. The results of the simulations showed some interesting trends. Increasing the power-law index leads to a significant reduction in the average Nusselt number of the cavity. Similarly, the corresponding flowfield behaviour resembles visually that which would have been obtained at a lower Rayleigh number in a Newtonian fluid. In Newtonian flow, this would indeed imply a reduction in heat transfer.

A flow feature, which has not been observed before, concerns the appearance of a triple vortex system in the cavity core, for highly shear-thinning fluids.

The lack of experimental data in the literature and the absence of similar numerical solutions prevents direct comparison of the results and hence quantitative assessment of accuracy. However, where analytical solutions exist (in isothermal cases) the method agrees well with theory, and the viscosity varies in accordance with the model prescribed. Further work is now in progress, to extend the method to time-dependent fluids.

ACKNOWLEDGEMENTS

The author would like to thank CHAM Limited of London for the use of the CFD code PHOENICS in this work.

REFERENCES

1 Markatos, N. C. and Pericleous, K. A. Laminar and turbulent natural convection in an enclosed cavity, *Int. J. of Heat and Mass Transfer*, **27**, 5 (1984)
2 Jones, I. P. A comparison problem for numerical methods in fluid dynamics: The 'double-glazing' problem, *Num. Meth. in Thermal Problems* (Ed. Lewis, R. W. and Morgan, K.), 338–348, Pineridge Press, Swansea, UK (1979)
3 De Vahl Davis, G. and Jones, I. P. Natural convection in a square cavity – a comparison exercise, *Int. J. Num. Methods in Fluids*, **3**, 227–248 (1983)
4 De Vahl Davis, G. Natural convection of air in a square cavity: A benchmark numerical solution, *Int. J. Num. Methods in Fluids*, **3**, 249–264 (1983)
5 Ostrach, S. Natural convection heat transfer in cavities and cells, *Proc. Int. Heat Transfer Conf.*, 365–379, Hemisphere, Washington, DC (1982)
6 Mallinson, G. D. and de Vahl Davis, G. Three dimensional natural convection in a box: A numerical study, *J. Fluid Mech.*, **83**, 1–31 (1977)
7 Fusegi, T., Farouk, B. and Kuwahara, K. 3-D natural convection-radiation interactions ij a differently heated cube, filled with GAs-soot mixtures, *Proc. Eurotherm 17*, Springer-Verlag, Portugal, 602–619 (1990)
8 Reizes, J. A., Leonardi, E. and de Vahl Davis, G. Natural convection near the density extremum of water, *Num. Meth. in Laminar and Turbulent Flow*, *Proc. 4th Int. Conf.*, 794–804 (Eds. Taylor, Olson, Gresho and Habashi), Pioeridge Press, Swansea (1985)
9 Maliska, C. R. and Milioli, F. E. A non-orthogonal model for the solution of natural convection problems in arbitrary cavities, *Num. Meth. in Laminar and Turbulent Flow*, Proc. 4th Int. Conf., 805–816 (Eds. Taylor, Olson, Gresho and Habashi), Pineridge Press, Swansea (1985)
10 Le Quere, P. and de Roquefort, T. A. Transition to unsteady convection of air in differently heated vertical cavities, *Num. Meth. in Laminar and Turbulent Flow*, *Proc. 4th Int. Conf.*, 841–852 (Eds. Taylor, Olson, Gresho and Habashi), Pineridge Press, Swansea (1985)
11 ASME WAM, Conf., Anaheim, Cal. (1992)
12 Akay, G. and Pericleous, K. A. The application of the PHOENICS computer code to non-Newtonian fluid flow: 3D modelling of a cavity transfer mixer, *Thermorheology of complex fluids*, Eurotherm seminar no. 5, Compiegne, France (1988)

13 Maeda, T. and Matsunaga, F. A survey note of non-Newtonian fluid flow simulation, *Proc. 3rd Int. PHOENICS User Conf.*, Dubrovnik, Yugoslavia (1989)
14 Maeda, T. and Murata, M. Visco-elastic flow simulation in rotating cylinders, *Physico-Chemical-Hydrodynamics J.*, **9**, 229 (1987)
15 Pericleous, K. and Patel, M. K. Industrial and environmental modelling of non-Newtonian fluid flows, *FED*, **145**, ASME WAM (1992)
16 Spalding, D. B. Mathematical modelling of fluid-mechanics, heat transfer and chemical reaction processes, A Lecture Course, CFDU Report, HTS/80/1, Imperial College, London (1980)
17 Bird, R. B., Stewart, W. E. and Lightfoot, E. N., *Transport Phenomena.* Wiley Int. (1960)
18 Metzner, A. B. *Handbook of Fluid Dynamics, Section 7* (Ed. Streeter, V. L.), McGraw-Hill, New York (1961)
19 Patankar, S. V. and Spalding, D. B. A calculation procedure for heat, mass and momentum transfer in three-dimensional parabolic flows, *Int. J. Heat Mass Transfer*, **15**, 1787 (1972)